First-principles estimation of partition functions representing disordered lattices such as the cubic phases of Li_2OHCl and Li_2OHBr

Jason Howard[*] and N. A. W. Holzwarth[†]
Department of Physics, Wake Forest University, Winston-Salem, North Carolina 27109-7507, USA

(Received 23 August 2018; published 16 January 2019)

In order to develop computational methods that can simulate thermodynamic properties of disordered materials at a first-principles level, we investigate the use of a random set of configurations to evaluate the canonical partition function of lattice-based disordered systems. Testing the sampling method on the one- and two-dimensional Ising models indicates that for the ordered system at low temperature, convergence is achieved when the number of samples $\mathcal{S}$ is comparable to or larger than the number of configurations Ω, while for the partially disordered system at high temperature, convergence is achieved for smaller sample sizes as low as $\mathcal{S} \approx \Omega/100$ or $\mathcal{S} \approx \Omega/1000$. The sampling method is combined with first-principles calculations to examine the ordered $\leftrightarrow$ disordered phase transition for the Li ion electrolyte materials Li_2OHCl and Li_2OHBr. Static-lattice internal energies and harmonic-phonon free energies were incorporated into the evaluation of the partition function. The evaluation of the partition function depends on the value of Ω corresponding to the number of metastable states of the system. Accordingly, we developed a method of approximating Ω using the properties of the sampled configurations. The results of the calculations are consistent with the experimental observation that the transition temperature for the orthorhombic $\leftrightarrow$ cubic phase transition is higher for Li_2OHCl than for Li_2OHBr. We expect the sampling method to be generally useful for investigating the thermodynamic properties of other disordered-lattice systems. We also investigate a "disordered-subspace function" which is shown to satisfy inequality relationships with respect to the Helmholtz free energy.

DOI: 10.1103/PhysRevB.99.014109

I. INTRODUCTION

When studying physical systems at finite temperatures, it is desirable to calculate thermodynamic quantities such as the internal energy, entropy, and corresponding Helmholtz free energy. Recently, there has been progress by several groups [1–5] in developing first-principles methods to include temperature-dependent effects including structural phase transitions. The detailed study of temperature-dependent properties of disordered materials at the first-principles level, however, remains a challenge. While cluster expansion models using parameters obtained from first-principles calculations [6–11] have successfully modeled phase stability including disorder in a variety of alloy and intercalation systems, not all systems of interest are amenable to cluster model representations. In this work, we investigate random-sampling techniques designed to work directly with first-principles methods to study disordered-lattice systems, including both static-lattice and lattice vibrational effects.

The motivation for developing these calculational methods came from studying the solid state electrolytes Li_2OHCl and Li_2OHBr [12–15]. These materials have been characterized as fast ion conductors and the material Li_2OHCl has been cycled in a symmetric cell with lithium metal electrodes [13]. An interesting aspect of these materials relates to their structural properties. Li_2OHCl is experimentally known [12] to exist in two phases: a disordered cubic phase ($T > 312$ K) and an ordered orthorhombic low-temperature phase ($T < 312$ K). The disordered cubic phase has superior ionic conductivity compared with the ordered phase and is the phase of interest for battery application. Interestingly, Li_2OHBr is only known [12] to exist in the disordered cubic phase. The question that detailed first-principles calculations can address is, "What causes the difference in the structural phase properties between these similar materials?"

The remainder of the paper is organized as follows. The general formalism is presented in Sec. II, including a discussion of evaluating the canonical partition function and Helmholtz free energy on the basis of exact configuration of the system in Sec. II A and on the basis of random sampling of the configurations in the system in Sec. II B. The sampling method is tested for one- and two-dimensional Ising models in Sec. III. The sampling method is then adapted to the first-principles study of the Li_2OHCl/Br system as described in Sec. IV. The so-called disordered-subspace approximation is introduced in Sec. V and results are compared with the sampled density of states method. The discussion and conclusions of the work are given in Sec. VI. Additional details of the results and formalism are given in Appendices A–C.

II. FREE-ENERGY FORMALISM

A. Exact configuration analysis

The materials properties that we wish to investigate require accurate estimates of the Helmholtz free energy:

$$F(T) \equiv -k_B T \ln[Z(T)], \tag{1}$$

[*]Present address: Materials Science Division, Argonne National Laboratory, Lemont, IL 60439, USA; jdhoward@anl.gov
[†]natalie@wfu.edu

where k_B denotes the Boltzmann constant, T denotes the temperature, and Z denotes the canonical partition function. For an ideal system having a finite number Ω of configurations represented by vectors $\{\mathbf{\Sigma}_i\}_\Omega$, each with their corresponding energies $\{e_i\}_\Omega$, it is possible to calculate the partition function according to

$$Z(T) = \sum_{i=1}^{\Omega} \exp\left(-\frac{e_i}{k_B T}\right) \equiv \sum_{j=1}^{\Pi} G_\Omega(E_j)\ \exp\left(-\frac{E_j}{k_B T}\right). \tag{2}$$

It will be convenient to assume that the configurations i are ordered so that $e_1 \leqslant e_i \leqslant e_\Omega$. Alternatively to explicitly enumerating each of the Ω energies, it is often convenient to analyze the energies in terms of a histogram $\mathcal{H}(E_j, \{e_i\}_\Omega) \equiv G_\Omega(E_j)$ evaluated at energies $\{E_j\}_\Pi$. The function $G_\Omega(E_j)$ is the density/number of states at energy E_j for our system which can be used in the evaluation of the partition function using the second expression in Eq. (2).

A system characterized by the Ω configurations and their energies $\{\mathbf{\Sigma}_i, e_i\}_\Omega$ represents the full thermodynamic range of a material having a particular lattice type. Systems having multiple structural phases need separate enumerations of their configurations and energies for each structure. For example, for the material systems of our study, Li_2OHCl and Li_2OHBr, the orthorhombic and cubic phases will be characterized separately.

B. Sampling analysis

The above analysis depends on the complete knowledge of the configurations and energies $\{\mathbf{\Sigma}_i, e_i\}_\Omega$ of the system. For convenience, we will refer to this set of configurations as the "master set." In practice, it is more often the case that this information is only available through sampling. In this work we use random or "simple" sampling [16]. For example, a random procedure could be used to choose $\mathcal{S}$ configurations and their energies $\{\mathbf{\Sigma}_s, e_s\}_\mathcal{S}$. In general, each sampled configuration $\mathbf{\Sigma}_s$ corresponds to a configuration $\mathbf{\Sigma}_i$ of the master set. In fact a given configuration i can appear in the sample set multiple (m_i) times. Since each configuration of the master set is equally probable, it follows that in the limit of a very large sample set,

$$\frac{m_i}{\mathcal{S}} \underset{\mathcal{S}\to\infty}{=} \frac{1}{\Omega}. \tag{3}$$

In practice, within a given computation it may be convenient to increase the sample size $\mathcal{S}$ by augmenting an existing set. For convenience, we will assume that any given sample set $\{\mathbf{\Sigma}_s, e_s\}_\mathcal{S}$ is ordered such that $e_1 \leqslant e_s \leqslant e_\mathcal{S}$ for $1 \leqslant s \leqslant \mathcal{S}$.

We now investigate how to use the sampled set $\{\mathbf{\Sigma}_s, e_s\}_\mathcal{S}$ to approximate the thermodynamic quantities of interest. It follows from Eq. (3) that a histogram function of the sampled set can be used to estimate the density of states:

$$\frac{G_\Omega(E_j)}{\Omega} \underset{\mathcal{S}\to\infty}{=} \frac{\mathcal{H}(E_j, \{e_s\}_\mathcal{S})}{\mathcal{S}} \equiv \frac{G_\mathcal{S}(E_j)}{\mathcal{S}}. \tag{4}$$

These equations can be used to estimate the partition function and Helmholtz free energy of the system. There is substantial literature detailing algorithms to estimate $G_\Omega(E_j)$ using more sophisticated sampling methods such as the Wang-Landau algorithm [16]. However, by assuming uniform random sampling, a reasonable approximation to the partition function can be determined at finite size $\mathcal{S}$ by a scaled summation over the sample set either by direct summation or through the histogram-sampled density of states:

$$\begin{aligned} Z(T) &\approx \frac{\Omega}{\mathcal{S}} \sum_{s=1}^{\mathcal{S}} \exp\left(-\frac{e_s}{k_B T}\right) \\ &= \frac{\Omega}{\mathcal{S}} \sum_{r=1}^{\mathcal{P}} G_\mathcal{S}(E_r)\ \exp\left(-\frac{E_r}{k_B T}\right). \end{aligned} \tag{5}$$

Here $\mathcal{P}$ denotes the number of distinct energies that appear in the sampled set. We will refer to this result as the "sampled density of states" (SDOS) analysis. Provided that we can estimate Ω and that the sample size $\mathcal{S}$ well represents the system, the SDOS estimate of the partition function can be used in Eq. (1) to estimate the Helmholtz free energy $F(T)$. The logic used to justify the sampling form of the canonical partition function given by Eq. (5) does not rely on how the energies are evaluated and should be equally valid for analyses of model Hamiltonian systems and for "first-principles" simulations.

III. TEST OF SAMPLING FORMALISM FOR MODEL SYSTEMS

Before applying the sampling methods to first-principles treatments of materials systems, it is prudent to test how these approximation techniques may work for well-known models such as the one-dimensional and two-dimensional Ising models in zero magnetic field.

A. One-dimensional Ising model

First a finite one-dimensional Ising model with n sites and free boundary conditions will be analyzed. In this case, each configuration $\mathbf{\Sigma}_i$ consists of a list of site values $\sigma_k^i = \pm 1$ for $1 \leqslant k \leqslant n$. The corresponding configuration energy is given by

$$e_i = -J \sum_{k=1}^{n-1} \sigma_k^i \sigma_{k+1}^i, \tag{6}$$

where J is the coupling constant. The exact free energy of this system per lattice site is given by [17]

$$\frac{F_{\text{exact}}(T,n)}{n} = -\frac{k_B T}{n} \ln\left[2^n \cosh^{n-1}\left(\frac{J}{k_B T}\right)\right]. \tag{7}$$

Here the Helmholtz free energy is scaled by the number of sites n.

For numerical testing, we chose the case with $J > 0$ and the number of sites to be $n = 16$, corresponding to $\Omega = 2^{16} = 65\,536$ as the number of configurations in the master list. The number of samples $\mathcal{S}$ to determine $\{e_s\}_\mathcal{S}$ for the sampling method were chosen to be $\mathcal{S} = \Omega/100$, $\Omega/10$, or Ω. A comparison of the free energies calculated with these different samples and using the sampled partition function Eq. (5) compared with the exact Helmholtz free energy determined from Eq. (7) is shown in Fig. 1. The results show that the sampling density of states calculated from Eq. (5) closely reproduces the exact analytical result particularly at larger

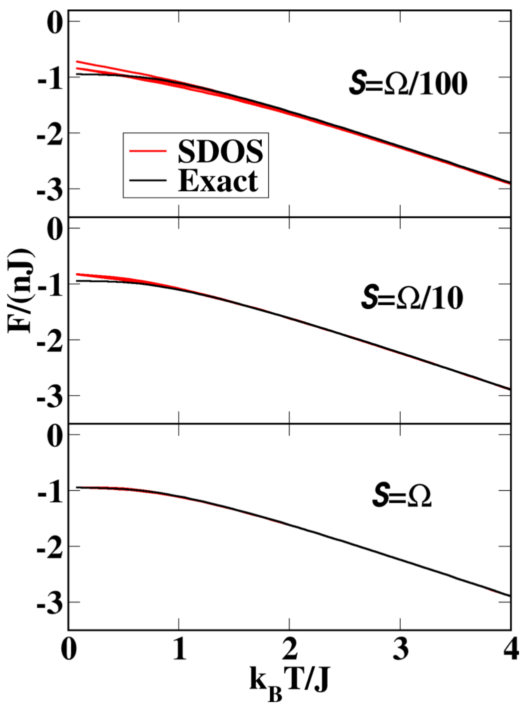

FIG. 1. Helmholtz free energy per lattice site as a function of the scaled temperature for the one-dimensional Ising model for $n = 16$, comparing the exact result ("Exact", black line) given by Eq. (7) with the sampling density of states ("SDOS", red lines) calculated from the sampled partition function Eq. (5). The sample sizes are $\mathcal{S} = \Omega/100$, $\Omega/10$, and Ω as indicated. Each calculation was repeated five times to show the variability.

temperatures even for $\mathcal{S} = \Omega/100$. We find that for smaller system sizes, the same trend is seen, but the sampling density of state results show larger fluctuations.

B. Two-dimensional Ising model

Another model system suitable for testing is the two-dimensional Ising model on a square lattice [17–19]. We consider the case of a finite square of length n in both dimensions with periodic boundary conditions. In this case, each configuration $\boldsymbol{\Sigma}_i$ consists of a list of site values $\sigma^i_{k,l} = \pm 1$ with $1 \leqslant k \leqslant n$ and $1 \leqslant l \leqslant n$ with $\sigma^i_{k,n+1} \equiv \sigma^i_{k,1}$ and $\sigma^i_{n+1,l} \equiv \sigma^i_{1,l}$. The corresponding configuration energy is given by

$$e_i = -J \sum_{k,l=1}^{n} \sigma^i_{k,l}\big(\sigma^i_{k+1,l} + \sigma^i_{k,l+1}\big). \tag{8}$$

Here we assume a positive coupling constant ($J > 0$) and the number of lattice sites is given by n^2. An analytical expression for the Helmholtz free energy per lattice site of an infinite two-dimensional square lattice ($n \to \infty$) was derived [17–19] to be

$$\lim_{n\to\infty} \frac{F_{\text{exact}}(T,n)}{n^2} = -\frac{k_B T}{\pi} \int_0^{\pi/2} d\theta \, \ln(\lambda(T)\{1 + [1 - \kappa(T)\cos^2\theta]^{1/2}\}), \tag{9}$$

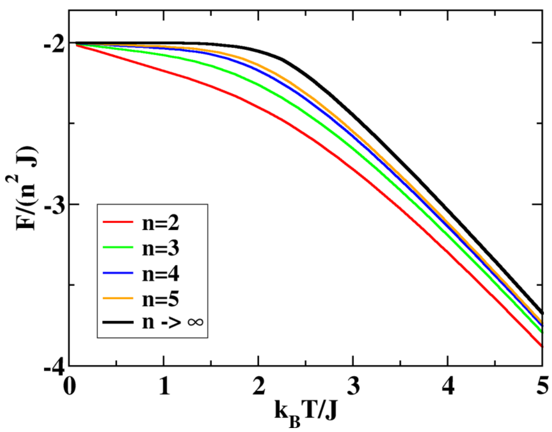

FIG. 2. Helmholtz free energy per lattice site as a function of the scaled temperature for the two-dimensional Ising model for various numbers of sites n in each of the two directions. The $n \to \infty$ result was evaluated from Eq. (9).

where

$$\lambda(T) \equiv 2\cosh^2\left(\frac{2J}{k_B T}\right) \quad \text{and} \quad \kappa(T) \equiv \left(\frac{2\tanh\left(\frac{2J}{k_B T}\right)}{\cosh\left(\frac{2J}{k_B T}\right)}\right)^2. \tag{10}$$

The variation of the Helmholtz free energy per lattice site as a function of scaled temperature is shown in Fig. 2 for various values of n including $n \to \infty$ evaluated from Eq. (9). Since the number of configurations for this model grows as $\Omega = 2^{n^2}$, it is practical to analyze finite systems using direct numerical evaluation or using our sampling methods up to $n = 5$.

The two-dimensional Ising model on the square lattice exhibits two different behaviors: ordered at low temperature and disordered at high temperature. The critical temperature T_c between these two regimes can be determined analytically for the infinite $n \to \infty$ limit:

$$\kappa(T_c) = 1 \quad \text{where} \quad \frac{k_B T_c}{J} \approx 2.269. \tag{11}$$

Another interesting aspect of the two-dimensional Ising model on a square lattice with periodic boundary conditions is the dependence of the free energy per lattice site as a function of lattice size n as illustrated in Fig. 2. This is an example of analyzing the supercell size dependence of this two-dimensional system. It is apparent from Fig. 2 that the free energy per lattice site for a finite-n system is less than its value in the $n \to \infty$ limit. In this case, it is reasonable to conclude that at low temperatures, entropic effects are overestimated for finite-n systems compared with the corresponding $n \to \infty$ case. For this model, the overestimation is due to the twofold degeneracy of the ground state of the supercell which contributes more entropy per lattice site for small supercells than for larger supercells.

For this two-dimensional Ising model we have the opportunity to investigate the convergence of the sampling size $\mathcal{S}$ for estimating the free energy using the sampling density of states from the sampled partition function Eq. (5). For testing, five calculations where performed for the $n = 5$ case for $\mathcal{S} = \Omega/10\,000$, $\Omega/1000$, $\Omega/100$, $\Omega/10$, and Ω. The results

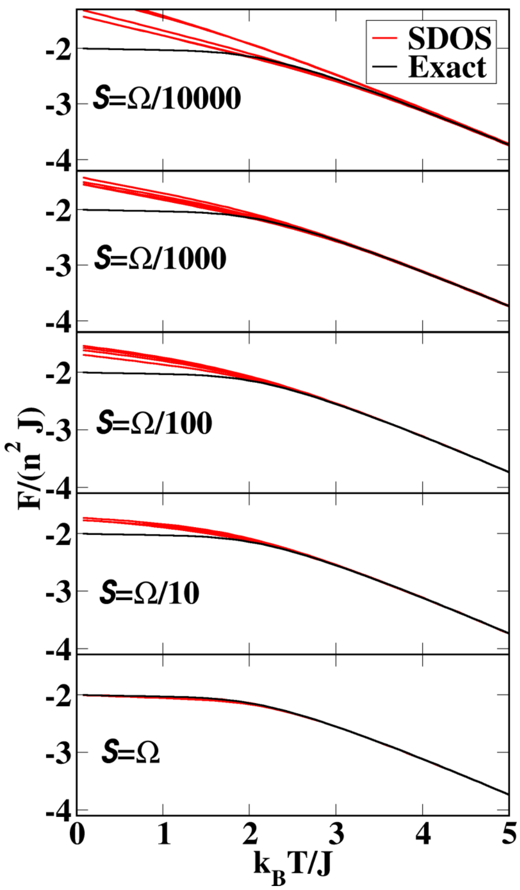

FIG. 3. Convergence of the free energy of the two-dimensional square Ising model for $n = 5$ with respect to number of samples $\mathcal{S}$, comparing sampling density of states ("SDOS", red lines) results from Eq. (5) with the exact result (black line). The sample sizes are $\mathcal{S} = \Omega/10\,000$, $\Omega/1000$, $\Omega/100$, $\Omega/10$, and Ω as indicated. Each calculation was repeated five times to show the variability.

are shown in Fig. 3. The results show that as the number of samples $\mathcal{S}$ increases, the 5 different calculations become closer to together and converge towards the $\mathcal{S} \to \infty$ limit. For the ordered phase with $T < T_c$, the results are well converged at a sample size of $\mathcal{S} = \Omega$, while for $T > T_c$ the results are well converged at $\mathcal{S} = \Omega/1000$.

IV. IMPLEMENTATION OF RANDOM-SAMPLING FORMALISM TO FIRST-PRINCIPLES SIMULATIONS

A. Configuration analysis for first-principles simulations of Li_2OHCl and Li_2OHBr

The materials of this study—Li_2OHCl and Li_2OHBr—have well-defined crystal structures, each of which can be adapted to discrete lattice models in order to enumerate their configurations $\{\mathbf{\Sigma}_i\}_\Omega$. In related previous work [15], we used a quasiharmonic approach to estimate the free energies of the structures, allowing the lattice parameters to vary within the analysis. However in the present work which focuses on systematic analysis of the order $\leftrightarrow$ disorder phase transition, we approximated each configuration with constant lattice parameters using the harmonic-phonon approximation [20]. Within this framework the energy of each configuration $\mathbf{\Sigma}_i$ can be determined as a sum of static-lattice and harmonic-phonon contributions:

$$e_i(T) = u_i^{\rm SL} + f_i^{\rm vib}(T). \tag{12}$$

Here $u_i^{\rm SL}$ denotes the static-lattice energy of configuration i calculated within density functional theory. The term $f_i^{\rm vib}(T)$ denotes the vibrational contributions to the Helmholtz free energy of the configuration i which is calculated within the harmonic-phonon approximation. Using density functional perturbation theory [20], the phonon density of states $g_i(\omega)$ for the configuration i is determined as a function of the phonon frequency ω. The explicit expression [21] for $f_i^{\rm vib}(T)$, which is derived from the quantum mechanical distribution of phonon states, takes the form

$$f_i^{\rm vib}(T) = k_B T \int_0^\infty d\omega g_i(\omega) \ln\left[2\sinh\left(\frac{\hbar\omega}{2k_B T}\right)\right]. \tag{13}$$

In this expression, the phonon density of states is normalized to $3M$, where M represents the number of atoms in the simulation cell. We note that with Eq. (12), the configuration energy $e_i(T)$ is temperature-dependent; while the static-lattice contribution $u_i^{\rm SL}$ is generally temperature-independent for the insulating materials of our study, the phonon contributions have a strong temperature dependence. This temperature-dependent form of $e_i(T)$ follows from the factorization of the system partition function into static-lattice and vibrational contributions according to

$$Z(T) = \sum_{i=1}^{\Omega} \exp\left(-\frac{u_i^{\rm SL}}{k_B T}\right) z_i^{\rm vib} = \sum_{i=1}^{\Omega} \exp\left(-\frac{u_i^{\rm SL} + f_i^{\rm vib}}{k_B T}\right), \tag{14}$$

where $z_i^{\rm vib} \equiv z_i^{\rm vib}(T)$ denotes the partition function of the vibrational modes of configuration i.

The challenge of this work is to study the order $\leftrightarrow$ disorder phase transitions in Li_2OHCl and Li_2OHBr as a function of T. Experimentally [12], the low-temperature ($T < 310$ K) phase of Li_2OHCl has been characterized as an ordered orthorhombic structure while the high-temperature phase is a disordered cubic structure. The experimental analysis [12] of Li_2OHBr finds only the disordered cubic structure for temperatures $T > 223$ K (corresponding to $T > -50\,^\circ$C). For this study, we will analyze both the orthorhombic and cubic structures of both materials. Two distinct sets of lattice configurations are used. For the ordered orthorhombic phase, only a single configuration ($\Omega^O = 1$), specified by a single set of coordinates and its energy $\{\mathbf{\Sigma}_1^O, e_1^O(T)\}$, is needed. For the disordered cubic phase a large number of configurations (Ω^c) with sets of coordinates and energies $\{\mathbf{\Sigma}_i^c, e_i^c(T)\}_{\Omega^c}$ are needed.

1. Analysis of ordered phases

The structures of ordered orthorhombic phases of Li_2OHCl and Li_2OHBr are not experimentally known in detail. In our previous work [15], we identified a candidate structure for the orthorhombic phase of Li_2OHCl which was consistent with experimental analysis of Schwering *et al.* [12] and with the experimental results reported in Ref. [15]. This structure, having 10 atoms per unit cell, is characterized

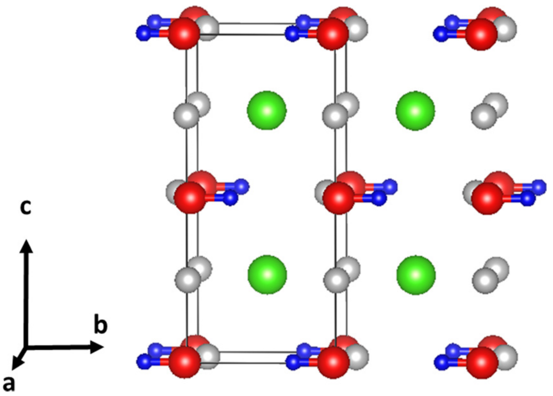

FIG. 4. Ball and stick diagram of O1 orthorhombic structure of Li_2OHCl having the space group $Pmc2_1$. The ball colors gray, red, blue, and green indicate Li, O, H, and Cl sites, respectively.

by the space group $Pmc2_1$ (No. 26) [22] with static-lattice optimized lattice parameters of $a = 3.831$ Å, $b = 3.617$ Å, and $c = 7.985$ Å which approximately map to $c/2, a$, and b reported by Schwering *et al.* [12]. We will reference this structure as O1. The structural details for this system are given in Ref. [15]. In the course of further study of this system we found a second candidate ground state structure (O2) having symmetry $Cmcm$ (No. 63) having 40 atoms per conventional unit cell with static-lattice optimized lattice parameters of $a = 7.91$ Å, $b = 7.74$ Å, and $c = 7.42$ Å which approximately map to the lattice parameters b, c, and $2a$ reported by Schwering *et al.* [12]. Ball and stick models of both of these structures are shown in Figs. 4 and 5. The lattice parameters for the O2 structure are listed in Table I. The x-ray patterns for the two candidate structures are both similar to the experimentally reported pattern as shown in Fig. 6. It is not unusual for the analysis of x-ray powder patterns to result in some structural ambiguity. On the basis of the x-ray powder diffraction patterns, the two structures appear to be very similar [23]. Since the lattice constants and the fractional coordinates for both oxygen and chlorine of the O1 and O2 structures are very similar, the similarity of the simulated x-ray patterns is not unexpected. However, the first-principles calculations using the harmonic-phonon

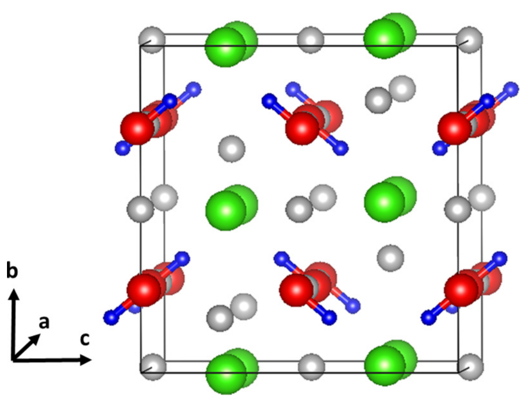

FIG. 5. Ball and stick diagram of O2 orthorhombic structure of Li_2OHCl having the space group $Cmcm$. The ball colors gray, red, blue, and green indicate Li, O, H, and Cl sites, respectively.

TABLE I. Optimized structural parameters for the O2 phases of Li_2OHCl and Li_2OHBr in the orthorhombic space group $Cmcm$ (No. 63). The corrected DFT-LDA lattice parameters for Li_2OHCl are $a = 7.91$, $b = 7.74$, and $c = 7.42$ Å and for Li_2OHBr are $a = 8.01$, $b = 8.03$, and $c = 7.88$ Å. The table lists the atomic site type, the multiplicity and Wyckoff label, and the x, y, and z fractional coordinates of the unique sites referenced to the conventional unit cell for Li_2OHCl and Li_2OHBr.

		Li_2OHCl			Li_2OHBr		
Atom	Wyckoff	x	y	z	x	y	z
O	8 f	0.000	0.747	0.510	0.000	0.741	0.513
H	8 f	0.000	0.831	0.407	0.000	0.824	0.419
Cl/Br	8 g	0.750	0.487	0.250	0.747	0.487	0.250
Li	8 d	0.250	0.250	0.000	0.250	0.250	0.000
Li	4 b	0.000	0.500	0.000	0.000	0.500	0.000
Li	4 c	0.000	0.167	0.250	0.000	0.197	0.250

approach find the ground state energy difference per formula unit to be $e_1^{O2} - e_1^{O1} = -0.02$ eV at $T = 0$ K and $e_1^{O2} - e_1^{O1} = -0.04$ eV at $T = 300$ K for Li_2OHCl, and $e_1^{O2} - e_1^{O1} = -0.06$ eV throughout the temperature range $0 \leqslant T \leqslant 300$ K for Li_2OHBr. This suggests that the O2 structure is more stable by an appreciable amount for both materials. Of course we are well aware that we have not exhausted all possible ordered orthorhombic structures. Consequently, both of the candidate orthorhombic structures are included in this study.

2. *Configuration analysis of disordered cubic phase*

A model of a unit cell of the disordered cubic phase is shown in Fig. 7. The space group of the structure is $Pm\bar{3}m$ (No. 221). The H sites have 4π radians of freedom about each O site and the Li ions randomly occupy two-thirds of their face-entered-cubic-like sublattice. In this case, the unit

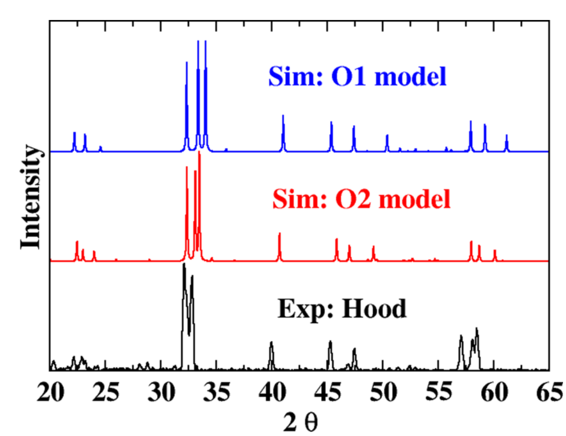

FIG. 6. Comparison of simulated and experimental x-ray diffraction patterns at wavelength $\lambda = 1.54056$ Å for the orthorhombic structure of Li_2OHCl. The experimental result was measured at room temperature by Zachary Hood. The simulated results were based on the the optimized O1 and O2 structures in the static-lattice approximation and generated using the Mercury [24] software package. The "Sim: O1 model" and "Exp: Hood" results were previously presented in Ref. [15].

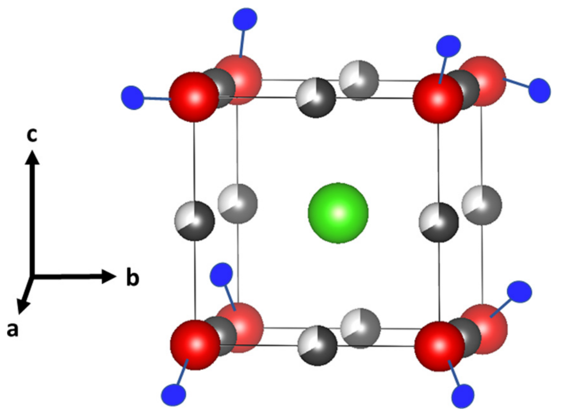

FIG. 7. Ball and stick model of a unit cell of the disordered cubic structure of Li_2OHCl and Li_2OHBr. Ball colors gray, red, blue, and green indicate Li, O, H, and Cl or Br sites, respectively. The shading of the Li sites indicates their fractional (two-thirds) occupancy.

cell contains one formula unit of Li_2OHCl/Br. Using the procedure described in Sec. IV B, we estimated the cubic lattice constants with the DFT-LDA corrected values to be $a = 3.87$ Å and $a = 4.02$ Å for Li_2OHCl and Li_2OHBr, respectively. These values compare well to the $a = 3.9103(1)$ Å and $a = 4.04626(3)$ Å values reported by Schwering *et al.* [12]. Using these cubic lattice parameters, the simulations are carried out within $n\times n\times n$ supercells. In this work, $n = 2$ was used, consistent with available computer resources.

In order to use the harmonic-phonon approximation of Eq. (12) to evaluate the configuration energies of the cubic phase $[e^c_i(T)]$, the corresponding configurations $(\mathbf{\Sigma}^c_i)$ must represent local equilibrium structures of the disordered lattice, taking into account both the fractional occupancies of the Li sublattice and the orientational disorder of the OH bonds. The challenge is to develop a scheme to enumerate the set of configurations and energies $\{\mathbf{\Sigma}^c_i, e^c_i(T)\}_{\Omega^c}$ corresponding to these local minima. In practice, these are evaluated by random sampling as formulated in Sec. II B, using the number of samples $\mathcal{S}^c$ consisting of configuration sets $\{\mathbf{\Sigma}^c_s, e^c_s(T)\}_{\mathcal{S}^c}$.

There are many ways to construct the random samples $\{\mathbf{\Sigma}^c_s, e^c_s(T)\}_{\mathcal{S}^c}$ of the metastable states of this system. In this work, the generation of the $\mathcal{S}^c$ configuration samples was achieved as follows. Initial structures were generated based on random occupation of the Li sublattice and OH bond orientations. For each initial structure, a nearby local minimum for the fixed supercell was found using the following two steps. In the first step, the Li positions were held fixed according to their sampled configuration while the structure was optimized by minimizing the static-lattice energy with respect to the other atomic positions. In the second step, the configuration was optimized with respect to all of the atomic positions. The resulting sample configuration $\mathbf{\Sigma}^c_s$ and its corresponding static-lattice energy $u^{\rm SL}_s$ could be assumed to represent a sample metastable state of the system. As detailed in Sec. IV B the two optimization steps could be performed with relaxed convergence criteria, as long as their accuracy was sufficient to identify the lowest energy structures. In practice, the number of samples processed in this way was chosen to be $\mathcal{S}^c = 10\,000$. The resultant values of the static-lattice internal energies $\{u^{\rm SL}_s\}$ are shown in Fig. 8 in histogram form.

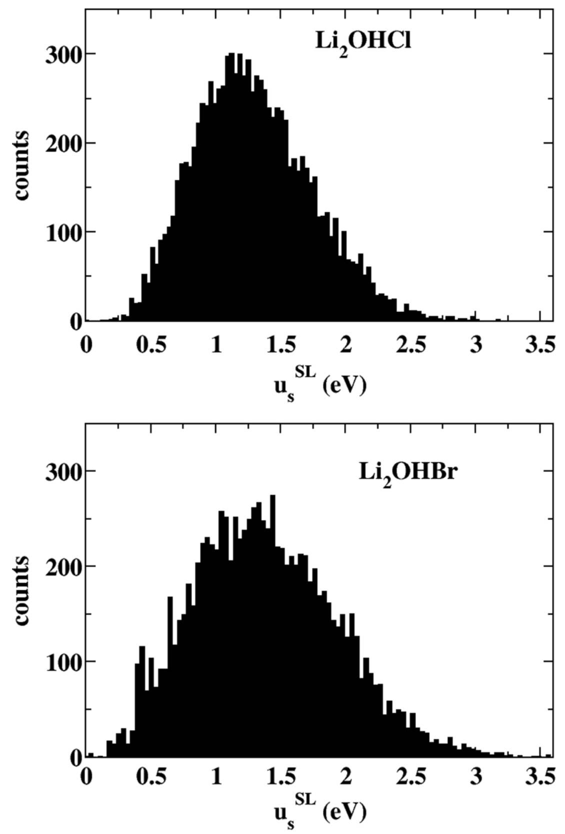

FIG. 8. Histogram plots of static-lattice internal energies $\{u^{\rm SL}_s\}_{\mathcal{S}^c}$ for the cubic phases of Li_2OHCl (upper panel) and Li_2OHBr (lower panel). The static-lattice energies are given relative to their lowest energy values and have units of eV/supercell. The histograms are normalized so that their integral is equal to $\mathcal{S}^c = 10\,000$. This sample set was constructed from randomly occupying the Li sublattice and randomly choosing the OH bond orientations in the $2\times2\times2$ simulation cell as described in the text.

Anticipating the evaluation of the partition function of the cubic phase using the sampling form Eq. (5), we note that for temperatures of interest ($T \leqslant 400$ K), the sampling energies that contribute are confined to the energies $e^c_s - e^c_1 \lesssim 0.2$ eV. This means that the summation maximum can be truncated to $s_{\rm max}$, where for this case, $s_{\rm max} \approx 20$. Accordingly, we then chose the $s_{\rm max}$ configurations corresponding to the $s_{\rm max}$ smallest values of $u^{\rm SL}_s$ to calculate their phonon spectra and their corresponding vibrational free energies $f^{\rm vib}_s(T)$. For these $s_{\rm max}$ configurations and for each temperature T, we can then form the ordered list of configuration energies $e_s(T) = u^{\rm SL}_s + f^{\rm vib}_s(T)$ to be used to evaluate the sampled partition function and corresponding Helmholtz free energy. The distribution of states for these $s_{\rm max}$ configurations is shown in Fig. 9 for the cubic phases of Li_2OHCl/Br. In this figure, both the static-lattice energies $\{u^{\rm SL}_s\}$ and harmonic-phonon approximate full energies $\{e_s(T)\}$ are presented for $T = 300$ K. Here we see that the effects of the vibrational energies $\{f^{\rm vib}_s\}$ are significant.

While we have reasonably argued that only the $s_{\rm max}$ lowest energy configurations are important for evaluating the

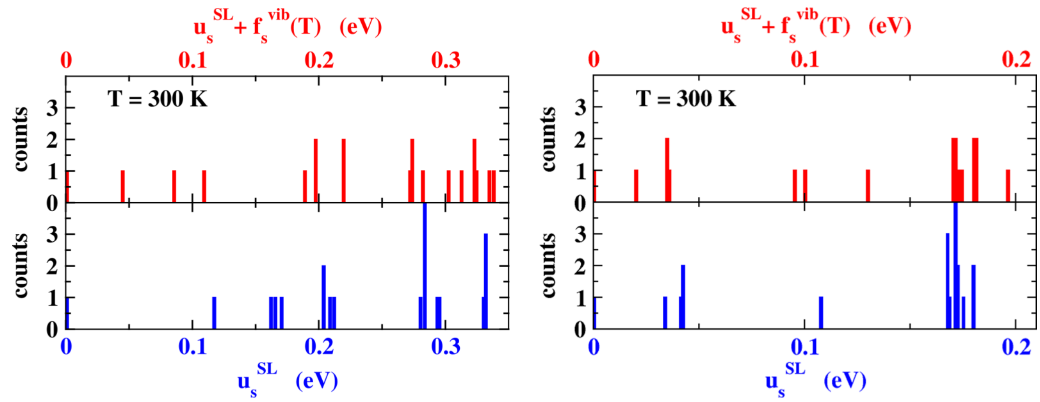

FIG. 9. Detailed plot of histograms shown in Fig. 8 for the sampled energies of the cubic phases of Li_2OHCl and Li_2OHBr. The lower blue panels show the 20 lowest static-lattice energies $\{u_s^{SL}\}$, while the upper red panels show the corresponding full energies $\{e_s(T) \equiv u_s^{SL} + f_s^{vib}(T)\}$ evaluated at $T = 300$ K. In each plot the energy scale is adjusted relative to u_1^{SL} or $e_1(T)$, as appropriate.

sampling partition function, it is still necessary to estimate the total number of metastable states Ω^c within the supercell. The details of this analysis are given in Appendices B and C. There it is explained that a given sample set $\{\mathbf{\Sigma}_s\}_{\mathcal{S}^c}$ can be characterized in terms of its number of duplicate pairs (counted twice) $d(\{\mathbf{\Sigma}_s\}_{\mathcal{S}})$ defined in Eq. (B2) which are listed in Table II. Appendix B also explains that if one has many sample sets of the same size $\mathcal{S}^c$ the average value depends on Ω^c according to Eq. (B1). Assuming that $d(\{\mathbf{\Sigma}_s\}_{\mathcal{S}}) \approx \langle d \rangle$, we can estimate Ω^c as listed in Table II. By constructing models of the configurations for the given number of samples $\mathcal{S}^c$, for calculated values of Ω^c, we can also estimate the error in the estimated values of Ω^c which are also listed in Table II.

As listed in Table II the estimate of Ω^c for the $n = 2$ supercells of Li_2OHCl and Li_2OHBr is roughly 10^7. Further analysis is needed to check whether this very large number of metastable states makes logical sense. We expect the number of configurations in this system to depend both on the Li sublattice occupation pattern and the OH bond orientations. Previously we have shown [15] that the cubic structure is characterized by a high degree of correlation between the Li vacancy configuration and the OH bond orientations. The number of configurations W^{Li} associated with the Li sublattice alone can be estimated by simply counting the number of ways of occupying two-thirds of the available sites in the supercell, so that

$$W^{Li} = \frac{(3n^3)!}{(2n^3)!(n^3)!}. \quad (15)$$

TABLE II. Estimated values of configuration parameters for $n\times n\times n$ supercell ($n = 2$) representing the cubic phase of Li_2OHCl and Li_2OHBr as detailed in Appendix B and Sec. II B, which also explains the quoted estimates of the expected errors in Ω^c.

	Li_2OHCl	Li_2OHBr
$d(\{\mathbf{\Sigma}_s\}_{\mathcal{S}^c})$	4	18
Calculated Ω^c	$(2.5 \pm 1.8)\times 10^7$	$(5.6 \pm 1.9)\times 10^6$
Assumed W^{Li}	7.4×10^5	7.4×10^5
Inferred w^H	1.6	1.3

For $n = 2$, the right-hand side of Eq. (15) is 7.4×10^5. While this estimate is based on the geometry of the ideal cubic structure before optimization to find metastable states, it is reasonable to assume that each ideal Li configuration is associated with a number of H configurations that optimize to form the master set of metastable configurations of the lattice $\{\mathbf{\Sigma}_s^c\}_{\Omega^c}$. This reasoning is consistent with the result that $\Omega^c > W^{Li}$. While we expect the number of H configurations that form metastable configurations to be different for each ideal Li configuration, it is reasonable to define an average number of H configurations W^H such that

$$\Omega^c = W^{Li} W^H. \quad (16)$$

Denoting the number of OH bond directions per formula unit as w^H, we expect that W^H scales as

$$W^H = (w^H)^{n^3}. \quad (17)$$

Using these relationships, we can infer that w^H is between 1 and 2 as listed in Table II, which is consistent with the geometry of the lattice. In particular, previous work on the cubic phase of Li_2OHCl [15] and similar studies of the cubic phase of Li_2OHBr show that the OH bonds tend to point either toward a nearby Li vacancy or between two neighboring Li vacancies. An approximate counting of the preferred OH orientations for this lattice gives a consistent estimate of w^H. These results also show that the sample size of $\mathcal{S}^c = 10\,000$ is quite small for this system, representing a small fraction (0.0001–0.001) of the estimated total number of configurations Ω^c. Given this large number of configurations for a supercell of $n = 2$, we expect that extending this analysis to larger supercells to represent this system is computationally prohibitive. From our analysis of finite-size errors shown in the two-dimensional Ising model results, we expect that our results overestimate the entropic contributions at low temperatures.

Having reasonably established that the cubic phase of the Li_2OHCl/Br system is characterized by a very large number of contributing configurations, it is difficult to take a look at the detailed structures. On the other hand, we can use the parameters defined in Appendices B and C to examine some of the properties of the configurations. The double number of

TABLE III. Values of Li sublattice parameters for evaluating the cubic phases of Li_2OHCl/Br for the configuration sample set with $\mathcal{S} = 10\,000$.

	Li_2OHCl	Li_2OHBr
$d(\{\mathbf{V}_s^{\rm init}\}_{\mathcal{S}})$	126	177
$d(\{\mathbf{V}_s^{\rm opt}\}_{\mathcal{S}})$	244	246
$C^{\rm same}$	4124	4278
$C^{\rm multiple}$	356	29

duplicate pairs of the ideal Li configurations in our sample, $d(\{\mathbf{V}_s^{\rm init}\}_{\mathcal{S}})$, is listed in Table III, showing values within the expected distribution of d values shown in the histogram of Fig. 15 in Appendix B. The corresponding values for the optimized Li configurations in our sample, $d(\{\mathbf{V}_s^{\rm opt}\}_{\mathcal{S}})$, are larger, which indicates that many of those initial configurations change during the optimization calculation. This behavior is expected given that each initial Li configuration is assigned a random H configuration, which may or may not be compatible with that geometry in the optimization calculation. In general, we expect that the likelihood of a given Li configuration existing within the optimized samples depends on how many associated H configurations there are. By calculating $C^{\rm same}$ for our samples, as listed in Table III, we find that 40% of the initial Li configurations remain the same after the optimization calculation. From the values of $C^{\rm multiple}$ listed in the table, of those configurations which change in the optimization set, only 4% and 0.3% contain doubly occupied Li sites for Li_2OHCl and Li_2OHBr, respectively.

B. Computational methods used in the first-principles simulations

The first-principles calculations described in this work were completed using density functional theory [25,26] simulations using the QUANTUM ESPRESSO code [27] within the projector augmented wave formalism [28] and using the local density approximation [29] for the exchange and correlation. It is well established [15,30] that these so-called DFT-LDA simulations do an excellent job of representing the static-lattice energies and the corresponding vibrational frequencies within the harmonic approximations, but tend to systematically underestimate the lattice parameters. Accordingly, all reported lattice parameter values are scaled by 1.02 in order to approximately compensate. In future work, it may be appropriate to reexamine the effects of the exchange-correlation functional form. The data sets for the projector augmented wave formalism basis and projector functions were produced with the ATOMPAW code [31]. Some of the data sets were improved (particularly Cl) by using the method of Sarkar *et al.* [32]. For calculations of the phonon densities of states, QUANTUM ESPRESSO was used to perform density functional perturbation theory calculations [20].

Several other computer packages were used in this study. To visualize and make figures of the crystal structures, VESTA [33] and XCRYSDEN [34] were used. Postprocessing of the static-lattice internal energies and phonon free energies was done with MATLAB [35]. Graphical representations of the results were constructed using the software package XMGRACE [36].

Care was taken to ensure that the calculations of this study were carried out with consistent and strict convergence parameters. This includes the plane wave cutoff of $|\mathbf{k}+\mathbf{G}|^2 \leqslant 64$ Ry. The $\mathbf{k}$-point sampling for Brillouin zone integration of the electronic wave functions used uniform grids with midpoint sampling, using $4\times4\times2$, $2\times2\times2$, and $2\times2\times2$ grids for the O1, O2, and $2\times2\times2$ supercell of the cubic structures, respectively. The $\mathbf{q}$-point sampling for Brillouin zone integration to determine the phonon density of states function $g_i(\omega)$ used uniform grids centered at the origin using $4\times4\times2$, $2\times2\times2$, and $2\times2\times2$ grids for the O1, O2, and $2\times2\times2$ supercell of the cubic structures, respectively.

For probing the disordered cubic structures of Li_2OHCl/Br, some additional computational techniques were used. First, the following procedure was used to estimate the cubic lattice parameters, following a similar method described in our previous work [15]. Specifically, $3\times3\times3$ supercells were used to generate 10 distinct configurations of the disordered Li sites and OH orientations which were each optimized with respect to the atomic positions and the cubic lattice parameter. The resulting averaged cubic lattice parameters were then used throughout the analysis of the free energy of this system. Second, in order to determine the sample set of 10 000 configurations, static-lattice calculations were performed using relaxed convergence parameters. In order to speed up the calculations the plane wave cutoff was reduced to $|\mathbf{k}+\mathbf{G}|^2 \leqslant 45$ Ry which resulted in sufficiently accurate static-lattice energies. Third, to evaluate the sampled partition function and corresponding Helmholtz free energy for temperatures $0 \leqslant T \leqslant 400$, we anticipated that only $s_{\max}$ lowest-energy states needed to be evaluated in detail. Therefore, the $s_{\max}$ configurations corresponding to the lowest static-lattice energies u_s^{SL} and their corresponding relaxed atomic coordinates were reoptimized using the strict convergence parameters and their phonon densities of states were calculated.

C. Evaluation of the Helmholtz free energies for Li_2OHCl and Li_2OHBr

Using the sampling partition function equations to estimate the Helmholtz free energy $F^c(T)$ for the cubic phases of Li_2OHCl and Li_2OHBr compared with the corresponding estimates $F^O(T)$ for their ordered orthorhombic phases, we are now in the position to calculate the free-energy differences

$$\Delta F(T) = F^c(T) - F^O(T). \tag{18}$$

The results are shown in Fig. 10 for the two candidate orthorhombic structures. The plots show that for both Li_2OHCl and Li_2OHBr the cubic phase is more stable than the O1 candidate orthorhombic structure throughout the temperature range. However, the results based on the O2 candidate orthorhombic structure do indicate a phase transition occurring 50 K higher in temperature for the Li_2OHCl structure compared with that of the Li_2OHBr structure. While the calculations underestimate the transition temperature compared with experimental results for Li_2OHCl, the qualitative behavior that the estimated temperature for the orthorhombic $\leftrightarrow$ cubic

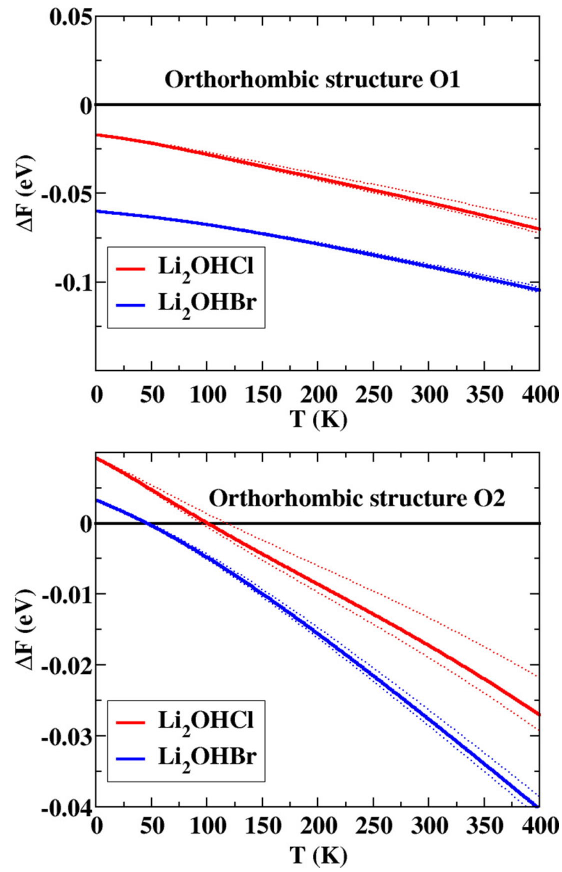

FIG. 10. Helmholtz free energy differences [Eq. (18)] in units of eV per formula unit of the disordered cubic and ordered orthorhombic phases of Li_2OHCl and Li_2OHBr. The upper and lower panels show ΔF based on the O1 and O2 orthorhombic structures, respectively. The full lines represent the values obtained using the Ω^c values given in Table II while the dashed lines indicate the range of values due to the estimated standard errors in the estimate of Ω^c.

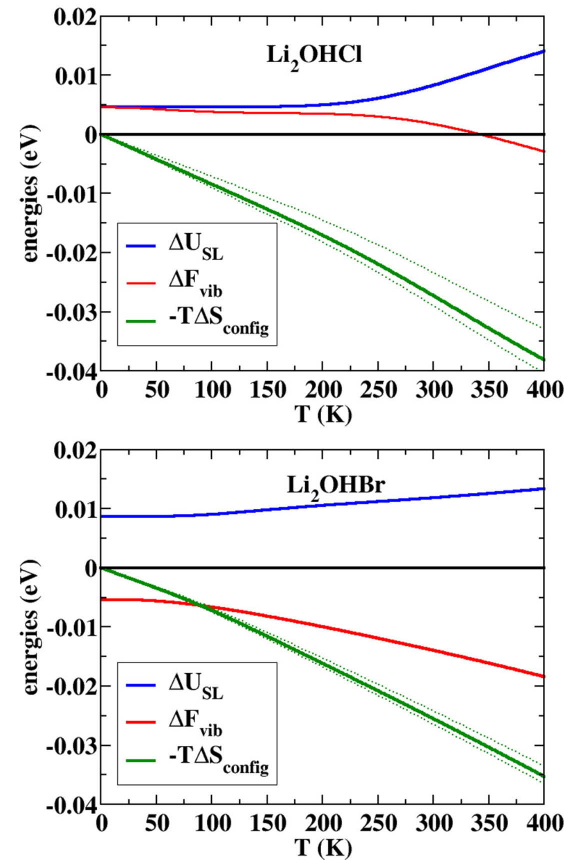

FIG. 11. Components of the free energy difference $\Delta F(T)$ for Li_2OHCl (upper panel) and Li_2OHBr (lower panel) given per formula unit, referenced to O2 orthorhombic structures of both materials, evaluated from Eq. (20). The full green lines were evaluated using the estimated values of Ω^c listed in Table II while the dashed green lines indicated the range of the estimated error in the estimate of Ω^c.

phase transition is considerably higher for Li_2OHCl than for Li_2OHBr.

It is useful to analyze the various components of the free-energy difference:

$$\Delta F(T) = \Delta U_{\mathrm{SL}} + \Delta F_{\mathrm{vib}}(T) - T\Delta S_{\mathrm{config}}(T). \tag{19}$$

Here all of the components are scaled per formula unit. The values for cubic phases are computed with the random sampling formalism and the values for the orthorhombic O2 phase are calculated with the corresponding single optimized configuration. Explicitly the contributions are given by

$$\begin{aligned}
\Delta U_{\mathrm{SL}} &= \left\langle \left(u_s^{\mathrm{SL}}\right)^c \right\rangle - \left(u_1^{\mathrm{SL}}\right)^{\mathrm{O2}}, \\
\Delta F_{\mathrm{vib}} &= \left\langle \left(f_s^{\mathrm{vib}}\right)^c \right\rangle - \left(f_1^{\mathrm{vib}}\right)^{\mathrm{O2}}, \\
T\Delta S_{\mathrm{config}} &= k_B T \ln[Z^c(T)] + \Delta U_{\mathrm{SL}} + \Delta F_{\mathrm{vib}}.
\end{aligned} \tag{20}$$

Here

$$\left\langle \left(u_s^{\mathrm{SL}}\right)^c \right\rangle = \frac{\sum_{s=1}^{s_{\max}} \left(u_s^{\mathrm{SL}}\right)^c \exp\left[-e_s^c/(k_B T)\right]}{\sum_{s=1}^{s_{\max}} \exp\left[-e_s^c/(k_B T)\right]} \tag{21}$$

and

$$\left\langle \left(f_s^{\mathrm{vib}}\right)^c \right\rangle = \frac{\sum_{s=1}^{s_{\max}} \left(f_s^{\mathrm{vib}}\right)^c \exp\left[-e_s^c/(k_B T)\right]}{\sum_{s=1}^{s_{\max}} \exp\left[-e_s^c/(k_B T)\right]}. \tag{22}$$

In this expression $s_{\max}$ denotes the number of states needed to converge the summation, $s_{\max} < 20$ in this case. Note that the configuration scaling factor Ω^c/S^c drops out of the analysis of the ΔU_{SL} and ΔF_{vib} energies, but does affect $\Delta S_{\mathrm{config}}$. The simulated results for these energies are given in Fig. 11 referenced to the O2 orthorhombic structure. Here it is seen that the ΔF_{vib} contributions seem to be largely responsible for stabilizing the cubic phase of Li_2OHBr at lower temperature than the corresponding contribution of Li_2OHCl.

V. DISORDERED-SUBSPACE APPROXIMATION

In the course of this investigation, an alternative approach which we call the "disordered-subspace approximation" (DSS) has emerged which may offer additional insight into the treatment of disordered systems.

A. Disordered-subspace formalism

The expressions given in Secs. II A and II B generally imply a large computational effort in summing over a large number of configurations. In practice, the free energy may be well approximated by evaluating expressions with a much smaller number of configurations. This is highlighted by the notion of a "disordered subspace" which contributes to the free energy. In this section we present both rigorous statements as well as relationships which result from our experience with many examples but which do not yet have a rigorous proof. In this section, we identify the latter type as "conjectures" or similar language.

The canonical partition function and the Helmholtz free energy as expressed in Sec. II A are very sensitive to temperature T. As $T \to 0$, only the lowest energy configuration contributes (assuming that the ground state is nondegenerate):

$$F(T=0) = e_1. \tag{23}$$

In this case, since a single configuration $\mathbf{\Sigma}_1$ characterizes the system, we can refer to the system as "fully ordered." In some cases, the fully ordered attribute may extend to higher temperatures, $T \geqslant 0$ K.

At the other extreme of the temperature range ($T \gg e_\Omega/k_B$), all of the configurations will contribute. The resulting "fully disordered" free energy can be written as

$$F_{fd}(T) = \frac{1}{\Omega}\sum_{i=1}^{\Omega} e_i - k_B T \ln(\Omega). \tag{24}$$

This form is derived by evaluating the partition function $Z(T)$ in the $T \to \infty$ limit, explicitly keeping the first two terms of a Taylor's expansion of $\ln[Z(T)]$ about $T \to \infty$. In Appendix A, we show that

$$F_{fd}(T) \geqslant F(T), \tag{25}$$

which means that at any temperature T, the expression for $F_{fd}(T)$ estimates an upper bound of the Helmholtz free energy $F(T)$ of the system.

The form of the fully disordered Helmholtz free energy given in Eq. (24) suggests a physical interpretation of the Helmholtz free energy in terms of a competition between the sum of configuration energies and the entropic contribution. It inspires a related estimate of Helmholtz free energy based on a subspace of the full set of configurations. Because the set of energies $\{e_i\}_\Omega$ are listed in ascending order $e_1 \leqslant e_i \leqslant e_\Omega$, it is convenient to choose the subspace as the first N energies in the set. The corresponding disordered-subspace free-energy function is defined by

$$F_{\rm dss}(T,N) = \frac{1}{N}\sum_{i=1}^{N} e_i - k_B T\left[\ln(\Omega) + \ln\left(\frac{N}{\Omega}\right)\right]. \tag{26}$$

Here the $\ln(\Omega)$ term cancels out of the equation, but it is convenient to keep it in this form. It is possible to show (Appendix A) that for any $N \leqslant \Omega$,

$$F_{\rm dss}(T,N) \geqslant F(T), \tag{27}$$

which means that $F_{\rm dss}(T,N)$ also estimates an upper bound of the Helmholtz free energy $F(T)$ of the system. Assuming a variational principle, it is conjectured that N_0, the value of N that minimizes $F_{\rm dss}(T,N)$ in Eq. (26), would be the best choice that gives the closest estimate of the Helmholtz free energy $F(T)$.

The notion of the "disordered-subspace" approach can be extended in terms of the sampled set $\{\mathbf{\Sigma}_s, e_s\}_\mathcal{S}$, analogous to the $F_{\rm dss}(T,N)$ function defined in Eq. (26) in terms of the master configuration set. We define a subspace kernel function which depends on $\mathcal{N} \leqslant \mathcal{S}$ of the lowest energy configurations according to

$$f(T,\mathcal{N},\mathcal{S}) \equiv \frac{1}{\mathcal{N}}\sum_{s=1}^{\mathcal{N}} e_s - k_B T\left[\ln(\Omega) + \ln\left(\frac{\mathcal{N}}{\mathcal{S}}\right)\right]. \tag{28}$$

Given this approximate form for the Helmholtz free energy, we expect that the optimal value would be obtained for the choice of $\mathcal{N} = \mathcal{N}_0$ that minimizes the subspace kernel:

$$f_0(T,\mathcal{N}_0,\mathcal{S}) = \min_{\mathcal{N}=\mathcal{N}_0}[f(T,\mathcal{N},\mathcal{S})]_{T,\mathcal{S}}. \tag{29}$$

For a given sample $\mathcal{S}$, the minimization is carried out separately for each evaluation temperature T. Because of the discrete formulation of the kernel $f(T,\mathcal{N},\mathcal{S})$, it follows that $\mathcal{N}_0(T)$ and $f_0(T,\mathcal{N}_0,\mathcal{S})$ are necessarily discontinuous functions. This analysis suggests a practical computational method to estimate the Helmholtz free energy as follows. Using random methods, a set of configuration samples $\{\mathbf{\Sigma}_s, e_s\}_\mathcal{S}$ is chosen to represent the system and the optimized subspace kernel $f_0(T,\mathcal{N}_0,\mathcal{S})$ is calculated according to Eq. (29) for each temperature T. This process can be repeated by augmenting the sampled set and reordering the entries so that $e_1 \leqslant e_s \leqslant e_\mathcal{S}$. It is expected that as the sample size grows, the results will converge to the optimized disordered-subspace function $F_{\rm dss}(T,N_0)$ and therefore to a good estimate of the Helmholtz free energy according to

$$F(T) \underset{\mathcal{S}\to\infty}{\approx} \frac{1}{\mathcal{N}_0}\sum_{s=1}^{\mathcal{N}_0} e_s - k_B T \ln\left(\frac{\mathcal{N}_0\Omega}{\mathcal{S}}\right). \tag{30}$$

It is interesting to consider the significance of the optimal number of sample contributions $\mathcal{N}_0$ determined in the disordered-subspace analysis of Eq. (29) for large sample sizes $\mathcal{S}$. The following discussion shows that $\mathcal{N}_0$ is connected with the number of microcanonical configurations $\mathcal{M}$ that describe the entropy of the system according to

$$S_\Omega = k_B \ln(\mathcal{M}). \tag{31}$$

This suggests the following relationship between the microcanonical configuration number $\mathcal{M}$ and $\mathcal{N}_0$:

$$\mathcal{M}(T) \approx \mathcal{N}_0(T)\frac{\Omega}{\mathcal{S}} \underset{\mathcal{S}\to\infty}{=} N_0(T), \tag{32}$$

using a notation to emphasize that $\mathcal{M}(T)$, $\mathcal{N}_0(T)$, and $N_0(T)$ vary with temperature T. Here $N_0(T)$ comes from the optimized value of N found in the exact configuration analog [Eq. (26)] of disordered-subspace kernel function Eq. (29).

B. Numerical examples of disordered-subspace approximation

It is useful to illustrate the relationships of the disordered-subspace formalism for the one-dimensional Ising model presented in Sec. III A. Figure 12 shows the results for a

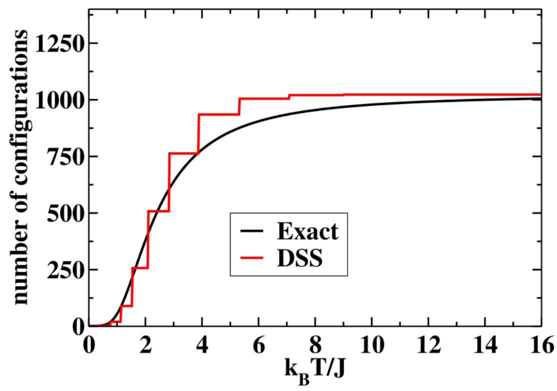

FIG. 12. Comparison of the number of microcanonical configurations $\mathcal{M}$, calculated from the analytic equations (black), and calculated from the disordered-subspace optimized value determined from the right-hand side of Eq. (32) (red), evaluated for the one-dimensional Ising model with $n = 10$, and sample size $\mathcal{S} = 10\Omega$.

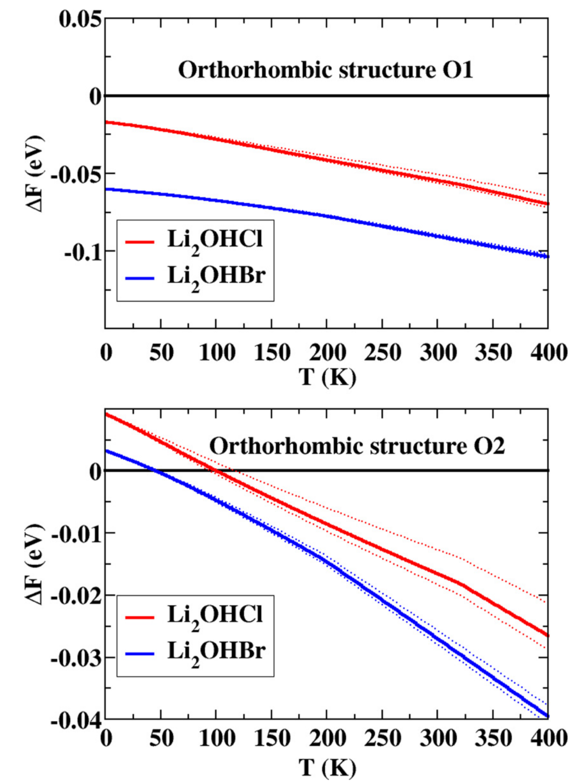

FIG. 13. Helmholtz free energy differences [Eq. (18)] in units of eV per formula unit of the disordered cubic and ordered orthorhombic phases of Li_2OHCl and Li_2OHBr analogous to results presented in Fig. 10 but evaluated within the disordered-subspace formalism.

one-dimensional Ising model with $n = 10$ sites, comparing $\mathcal{M}(T)$ calculated from Eq. (31) using analytic expressions of the finite one-dimensional Ising model to evaluate $S_\Omega = \langle e_i \rangle / T + k_B \ln Z$, with the approximate values determined from the right-hand side of Eq. (32), evaluated with sample size $\mathcal{S} = 10\Omega$. Here, $\langle e_i \rangle$ represents the canonical average of the configuration energies. The plot for the disordered-subspace analysis is shown as discontinuous due to the discrete nature of $\mathcal{N}_0(T)$ as it is formulated in terms of the disordered-subspace kernel in Eq. (29). Apart from these discontinuities, the results show good agreement with the exact value.

In addition to applying the disordered-subspace approximation to model systems, it can also be applied to the analysis of real materials. It is possible to use the disordered-subspace formalism as described in Sec. V to approximate the free energy differences between the cubic and orthorhombic phases analogous to the results presented in Sec. IV C. These results are shown in Fig. 13 for the $\Delta F(T)$ and in Fig. 14 for the component contributions. The results are qualitatively close to the analogous results shown in Figs. 10 and 11 evaluated using the sampled density of states analysis. The disordered-subspace analysis also allows us to estimate the corresponding number of microcanonical configurations $\mathcal{M}$ of the cubic structure, which, according to Eq. (32), is found to be roughly 10^3 for $2\times2\times2$ supercells of both Li_2OHCl and Li_2OHBr.

VI. DISCUSSION AND CONCLUSIONS

It remains a challenge to directly adapt first-principles methods, which have proven very successful in describing the detailed properties of ordered materials at low temperature, to simulate the effects of disorder and finite temperature. In this work, we have made some progress in developing and testing general lattice based methods for simulating disordered materials at finite temperature, using the order ↔ disorder phase transitions in Li_2OHCl/Br as an interesting model system.

We use random-sampling methods to evaluate the canonical partition function using Eq. (5). For Ising model tests, this method was found to converge well to the exact answer when the sample size $\mathcal{S}$ was comparable to or greater than the number of system configurations Ω, even at low temperatures. For higher temperatures and especially for temperatures above T_c in the two-dimensional Ising model, we find that the sampling results converge much more rapidly, finding accurate results for sample sizes as small as $\mathcal{S} \approx \Omega/100$ or $\mathcal{S} \approx \Omega/1000$ for the particular systems we examined. For studying systems in which the size of Ω is unknown, we demonstrated that the examination of the configuration vectors $\{\mathbf{\Sigma}_s\}_\mathcal{S}$ can provide a good estimate of Ω. In particular, the double number of duplicate pairs $d(\{\mathbf{\Sigma}_s\}_\mathcal{S})$ defined by Eq. (B2) can be calculated. Using Eq. (B1), the average value $\langle d \rangle$ can be used to estimate Ω. While the calculations improve with increasing sample sizes (as $\mathcal{S} \to \infty$), statistical methods can be used to estimate the error of the estimate of Ω. We introduced the "disordered-subspace" formalism which calls attention to the fact that as a function of temperature T, a subspace $\mathcal{N}_0(T)$ of the full $\mathcal{S}$ samples and correspondingly $N_0(T)$ configurations of the master set Ω contribute to the free energy approximated by Eq. (30). While this approach may or may not be competitive with directly evaluating the sampled canonical partition function through Eq. (5), the notion of the disordered-subspace approximation leads to an explicit estimate of the configurational entropy of the system using Eqs. (31) and (32).

The random-sampling methods together with first-principles methods were developed to studying the order ↔ disorder phase transition for the Li_2OHCl/Br system. While

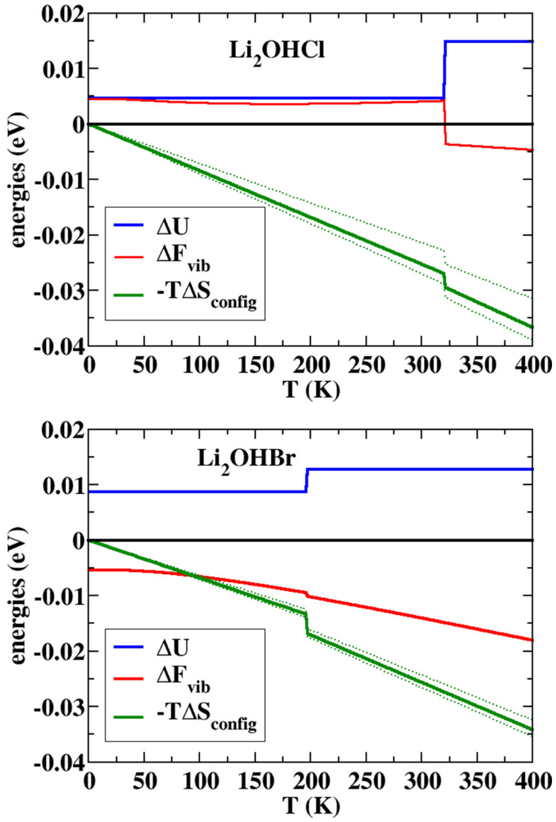

FIG. 14. Components of the free energy difference $\Delta F(T)$ for Li_2OHCl (upper panel) and Li_2OHBr (lower panel) given per formula unit, referenced to O2 orthorhombic structures of both materials, analogous to the results presented in Fig. 11 but evaluated within the disordered-subspace formalism.

we initially thought that the sample size of $\mathcal{S} = 10\,000$ was quite large, it turned out to be quite small compared with the estimated value of master configurations of $\Omega \approx 10^7$ in the cubic phase. While we expect that increased sampling will improve the results, the current sample size is nevertheless reasonable. By using reduced plane wave cutoff parameters in the initial optimization steps for finding the metastable state configurations and their corresponding static-lattice energies, the simulation was entirely feasible within our computational resources. This enabled us to choose a much smaller number of samples $s_{\max}$ for performing higher-accuracy optimizations and for evaluating the vibrational contributions shown in Fig. 9. The results shown in Fig. 10 indicate that the transition temperature occurs at a higher temperature for Li_2OHCl than for Li_2OHBr by 50 K, assuming the orthorhombic structure having *Cmcm* symmetry (O2) as the reference. The fact that the cubic phase is more stable than the O1 orthorhombic structure throughout the full temperature range gives further evidence that the O2 structure is more likely to be the physical structure of the orthorhombic phase of Li_2OHCl. Since no orthorhombic phase has been observed for Li_2OHBr, there is presently no experimental evidence to suggest either choice. The decomposition of the free energy differences into the various contributions shown in Fig. 11 indicates that the vibrational free energy difference is largely responsible for stabilizing the cubic phase in Li_2OHBr.

In performing the first-principles simulations for Li_2OHCl/Br, one can ask whether the particular choice of sampling construction is providing a good representation of the cubic phase configuration space. While it is not possible to answer that question directly, the analysis of the configuration parameters given in Sec. II B suggests that the properties of the metastable configurations are supportive of the notion that the range of metastable configurations of the cubic lattice was uniformly sampled.

The results for the Li_2OHCl/Br system encourage further development of these techniques and tools for studying the thermodynamic properties of a wide variety of disordered-lattice systems in terms of sets of random samples. This system exemplifies a case where random-sampling methods are preferable to cluster expansion approaches. The particular geometry of this system with two interdependent disordered components of the Li sublattice and the variable nearby OH bond angles is difficult to treat with a cluster expansion. In addition, the random-sampling method allows for the straightforward inclusion of both vibrational effects together with static-lattice effects in the energy analysis.

ACKNOWLEDGMENTS

This work was supported by NSF Grant No. DMR-1507942. Computations were performed on the Wake Forest University DEAC cluster, a centrally managed resource with support provided in part by the University. We would like to thank Dr. Zachary Hood from the Electrochemical Materials Laboratory at MIT for introducing us to these interesting materials and for his continued consultation. We would also like to thank Dr. Kanchan Sarkar from Materials Science and Engineering and Earth and Environmental Sciences at Columbia University for providing an atomic data set for Cl used in this study.

APPENDIX A: PROOF OF INEQUALITIES SHOWING THAT $F_{fd}(T)$ AND $F_{dss}(T)$ PROVIDE AN UPPER BOUND TO THE HELMHOLTZ FREE ENERGY

In order to prove the two inequalities given in Eq. (25) and Eq. (27), we consider the general equations with $N \leqslant \Omega$. The inequality that must be demonstrated can be written

$$\frac{1}{N}\sum_{i=1}^{N} e_i - k_B T \ln(N) \geqslant -k_B T \ln\left[\sum_{i=1}^{\Omega} \exp\left(-\frac{e_i}{k_B T}\right)\right]. \tag{A1}$$

This can be rearranged to the form

$$\frac{1}{N}\sum_{i=1}^{N}\left(-\frac{e_i}{k_B T}\right) \leqslant \ln\left[\frac{1}{N}\sum_{i=1}^{\Omega} \exp\left(-\frac{e_i}{k_B T}\right)\right]. \tag{A2}$$

Since the energies are ordered $e_1 \leqslant e_i \leqslant e_\Omega$, it follows that

$$\sum_{i=1}^{\Omega} \exp\left(-\frac{e_i}{k_B T}\right) \geqslant \sum_{i=1}^{N} \exp\left(-\frac{e_i}{k_B T}\right). \tag{A3}$$

Consequently, if the proof is completed in Eq. (A2) with the summation to Ω replaced by a summation to N, the original inequality [Eq. (A1)] is also true. Using the abbreviation for the positive real numbers $X_i \equiv \exp(-e_i/k_BT)$, and taking the exponential of both sides of the modified version of Eq. (A2), the inequality becomes

$$\left(\prod_{i=1}^{N} X_i\right)^{\frac{1}{N}} \leqslant \frac{1}{N}\sum_{i=1}^{N} X_i, \tag{A4}$$

which states that the geometric mean of a set of positive real numbers X_i is less than or equal to its arithmetic mean [37]. This result then provides the justification for Eqs. (25) and (27) and shows the utility of the disordered-subspace function.

APPENDIX B: DETAILS OF RELATIONSHIPS BETWEEN CONFIGURATIONS AND THEIR SAMPLING STATISTICS

While the exact value of the number of metastable states Ω which characterize the disordered system is not known, it is possible to estimate its value from characteristics of its $\mathcal{S}$ samples. We want to explore the relationship of the exact set of configurations $\{\mathbf{\Sigma}_i\}_\Omega$ and the sample set $\{\mathbf{\Sigma}_s\}_\mathcal{S}$. While each of the exact configurations $\mathbf{\Sigma}_i$ is unique, some of the sample configurations $\mathbf{\Sigma}_s$ may be duplicated. It can be shown that for a given system of Ω metastable states, the average number of duplicate pairs (doubly counted) for a set of size $\mathcal{S}$ is given by

$$\langle d\rangle = \frac{\mathcal{S}(\mathcal{S}-1)}{\Omega}. \tag{B1}$$

We note that this equation is consistent with Eq. (3) in the limit of $\mathcal{S} \to \infty$. The averaging in Eq. (B1) is performed over distinct sets $\{\mathbf{\Sigma}_s\}_\mathcal{S}$ for fixed size $\mathcal{S}$. For a given set, $\{\mathbf{\Sigma}_s\}_\mathcal{S}$, it is possible to calculate the double number of duplicate pairs using a Kronecker delta function according to

$$d(\{\mathbf{\Sigma}_s\}_\mathcal{S}) = \sum_{s=1}^{\mathcal{S}}\sum_{r(\neq s)=1}^{\mathcal{S}} \delta_{\mu_{sr},1}, \tag{B2}$$

where the duplicate measure function μ_{sr} is constructed to have the property

$$\mu_{sr}\begin{cases} =1, & \text{for } \mathbf{\Sigma}_s = \mathbf{\Sigma}_r, \\ \neq 1, & \text{for } \mathbf{\Sigma}_s \neq \mathbf{\Sigma}_r. \end{cases} \tag{B3}$$

In order to demonstrate this relationship, we can consider an analysis of the ideal Li sublattice of the Li_2OHCl/Br system. It is convenient to define occupation vectors $\mathbf{V}_s$. For the $n\times n\times n$ unit cell, the vector would have $K = 3n^3$ components. Expressing $\mathbf{V}_s$ in row vector form:

$$\mathbf{V}_s = [o_1^s, o_2^s, \ldots, o_K^s], \tag{B4}$$

where

$$\sum_{k=1}^{K} o_k^s = \frac{2}{3}K = 2n^3 \equiv L. \tag{B5}$$

For the ideal Li sublattice, the occupation numbers $\{o_k^s\}$ are all 0 or 1. However, in anticipation of using this formalism for the optimized supercell system as well, we can generalize the analysis to allow for the site occupations of $o_k^s > 1$ as well. For this vector construction, we can then define the duplicate measure function to be a modified vector dot product of the form

$$\mu_{sr} \equiv \frac{1}{L}\sum_{k=1}^{K}\sqrt{o_k^s o_k^r}. \tag{B6}$$

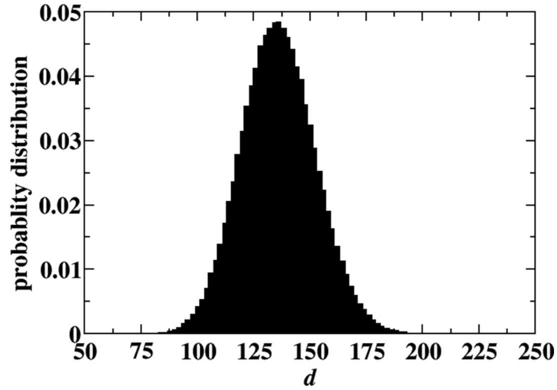

FIG. 15. Histogram of duplicate pair values (doubly counted) d for 512 000 sets of configurations $\{\mathbf{V}_s\}_\mathcal{S}$ for sample size $\mathcal{S} = 10\,000$ representing the ideal Li sublattice of the Li_2OHCl/Br system for $n = 2$ supercells.

In order to check the evaluation of Eqs. (B1) and (B2) for a representative system, we generated a large number ($Q = 512\,000$) of sets of samples having $\mathcal{S} = 10\,000$ configurations based on the configuration vectors $\{\mathbf{V}_s\}_\mathcal{S}$ representing the ideal Li sublattice for $n = 2$ supercells. The master set of configurations for this system (Ω) is given by the right-hand side of Eq. (15). For each of the Q sample sets, we calculated the value of d using Eq. (B2) and the histogram of the results is presented in Fig. 15. The distribution of d values appears to have a Gaussian shape with an average value of $\langle d\rangle = 135.969 \pm 0.023$. Here we have taken the error estimate as the standard deviation of the mean calculated as the standard deviation of the d values divided by $\sqrt{Q}$. The standard deviation of d itself ($\sigma_d \approx 16$) provides a good estimate of the error in evaluating the double number of duplicate pairs for this system with a single sample set. Using the known values of Ω and $\mathcal{S}$ for this system, the right-hand side of Eq. (B1) estimates $\langle d\rangle = 135.954$. This numerical test helps validate Eq. (B1).

APPENDIX C: DETAILS OF CONFIGURATION ANALYSIS FOR CUBIC PHASES OF Li_2OHCl/Br

In order to extend the analysis of Appendix B to a more realistic representation of the cubic phase of our system there are several considerations. Generally we assume that each initial configuration of the ideal cubic lattice maps, after optimization, to some metastable configuration that can be used in our analysis, generally maintaining the statistical sampling properties. We can develop some tools to assess this assumption and to estimate the total number of metastable configurations Ω^c. These tools will represent the Li sublattice using a generalization of Eq. (B4) and the full lattice coordinates, including the alternative H positions.

In practice, a single sample configuration set $\{\mathbf{\Sigma}\}_\mathcal{S}^{\text{init}} \to \{\mathbf{\Sigma}\}_\mathcal{S}^{\text{opt}}$ with sample size $S = 10\,000$ was constructed as described in Sec. IV B for evaluating the Helmholtz free energy.

First, consider the properties of the Li sublattice of these configurations. For this purpose, the idealized Li sublattice described in Appendix B must be generalized. While the configuration vectors $\{\mathbf{V}_s^{\text{init}}\}_{\mathcal{S}}$, defined in Eq. (B4), with the occupancy numbers $(o_k^s)^{\text{init}}$ having values of 0 or 1, well represent the initial configuration of the Li sublattice, after the optimization step, these configurations may change. Using an algorithm which assigns each Li to its nearest ideal site to define the occupation numbers $(o_k^s)^{\text{opt}}$ having values $0, 1, 2, \ldots$, we can construct corresponding configuration vectors $\{\mathbf{V}_s^{\text{opt}}\}_{\mathcal{S}}$ to represent the Li sublattice of the metastable states. Here, occupation values $(o_k^s)^{\text{opt}} > 1$ can occur when site k is occupied by two or more Li ions. These can be used to evaluate the double number of duplicate pairs according to Eq. (B2) $d(\{\mathbf{V}_s^{\text{init}}\}_{\mathcal{S}})$ and $d(\{\mathbf{V}_s^{\text{opt}}\}_{\mathcal{S}})$, representing the initial and optimized Li sublattice configurations, respectively. We can also count how many of the $\mathcal{S}$ configurations keep the same Li sublattice configuration after the optimization step compared with its initial configuration by evaluating

$$C^{\text{same}} = \sum_{s=1}^{\mathcal{S}} \delta_{\nu_{ss},1}, \quad \text{where } \nu_{ss} \equiv \frac{1}{L}\sum_{k=1}^{K}\sqrt{\left(o_k^s\right)^{\text{init}}\left(o_k^s\right)^{\text{opt}}}. \tag{C1}$$

Similarly, we can count how many of the $\mathcal{S}$ configurations have multiple occupancies on the Li sublattice sites by evaluating

$$C^{\text{multiple}} = \mathcal{S} - \sum_{s=1}^{\mathcal{S}} \delta_{\lambda_{ss},1}, \quad \text{where } \lambda_{ss} \equiv \frac{1}{L}\sum_{k=1}^{K}\left[\left(o_k^s\right)^{\text{opt}}\right]^2. \tag{C2}$$

The results of these parameters are summarized in Table III.

In order to extend the analysis of the atomic configurations beyond that of the Li sublattice, we need to consider the full set of atomic positions $\{\mathbf{R}_a^s\}$ where the atomic index a enumerates all of the M atoms in the supercell. In this case, the duplicate measure function needed to evaluate Eq. (B2) could be calculated from

$$\mu_{sr} = 1 + \sum_{a=1}^{M}\left|\mathbf{R}_a^s - \mathbf{R}_a^r\right|. \tag{C3}$$

In practice, a constant shift vector must often be added to this expression to account for a possible uniform drift of the coordinate system during the simulations. Typically, the evaluation of Eq. (C3) was performed with an error tolerance of 0.01 Å for each of the three directions of the position vectors $\mathbf{R}_a^s$. This form was used to evaluate $d(\{\boldsymbol{\Sigma}_s\}_{\mathcal{S}^c})$ listed in Table II.

[1] R. Bianco, I. Errea, L. Paulatto, M. Calandra, and F. Mauri, Phys. Rev. B **96**, 014111 (2017).
[2] R. Bianco, I. Errea, M. Calandra, and F. Mauri, Phys. Rev. B **97**, 214101 (2018).
[3] J. S. Bechtel and A. Van der Ven, Phys. Rev. Mater. **2**, 025401 (2018).
[4] J. B. Haskins and J. W. Lawson, J. Appl. Phys. **121**, 205103 (2017).
[5] C. Cazorla, D. Alfè, and M. J. Gillan, Phys. Rev. B **85**, 064113 (2012).
[6] D. de Fontaine, in *Cluster Approach to Order-Disorder Transformations in Alloys*, edited by H. Ehrenreich and D. Turnbull, Solid State Physics (Academic Press, New York, 1994), Vol. 47, pp. 33–176.
[7] P. D. Tepesch, G. D. Garbulsky, and G. Ceder, Phys. Rev. Lett. **74**, 2272 (1995).
[8] A. Van der Ven and G. Ceder, Phys. Rev. B **71**, 054102 (2005).
[9] R. Grau-Crespo, S. Hamad, C. R. A. Catlow, and N. H. de Leeuw, J. Phys.: Condens. Matter **19**, 256201 (2007).
[10] G. Sai Gautam, P. Canepa, A. Abdellahi, A. Urban, R. Malik, and G. Ceder, Chem. Mater. **27**, 3733 (2015).
[11] N. S. Harsha Gunda, B. Puchala, and A. Van der Ven, Phys. Rev. Mater. **2**, 033604 (2018).
[12] G. Schwering, A. Hönnerscheid, L. van Wüllen, and M. Jansen, Chem. Phys. Chem. **4**, 343 (2003).
[13] Z. D. Hood, H. Wang, A. Samuthira Pandian, J. K. Keum, and C. Liang, J. Am. Chem. Soc. **138**, 1768 (2016).
[14] Y. Li, W. Zhou, S. Xin, S. Li, J. Zhu, X. Lü, Z. Cui, Q. Jia, J. Zhou, Y. Zhao, and J. B. Goodenough, Angew. Chem., Int. Ed. Engl. **55**, 9965 (2016).
[15] J. Howard, Z. D. Hood, and N. A. W. Holzwarth, Phys. Rev. Mater. **1**, 075406 (2017).
[16] D. P. Landau and K. Binder, *A Guide to Monte Carlo Simulations in Physics*, 4th ed. (Cambridge University Press, Cambridge, 2015).
[17] B. M. McCoy and T. T. Wu, *The Two-Dimensional Ising Model* (Harvard University Press, Cambridge, MA, 1973).
[18] L. Onsager, Phys. Rev. **65**, 117 (1944).
[19] R. Baxter, *Exactly Solved Models in Statistical Mechanics* (Academic Press Inc., San Diego, CA, 1982).
[20] S. Baroni, S. de Gironcoli, A. Dal Corso, and P. Giannozzi, Rev. Mod. Phys. **73**, 515 (2001).
[21] A. A. Maradudin, E. W. Montroll, G. H. Weiss, and I. P. Ipatova, *Theory of Lattice Dynamics in the Harmonic Approximation*, 2nd ed. (Academic Press, New York, 1971).
[22] T. Hahn, editor, *International Tables for Crystallography, Volume A: Space-Group Symmetry*, 5th ed. (Kluwer Academic, Dordrecht, 2002). The symmetry labels used in this work are all based on this reference.
[23] In Ref. [15] we were able to use the quasiharmonic approximation [38] to approximate temperature-dependent lattice expansion effects which improved the agreement of the O1 structure with experiment. Preliminary similar treatment of the O2 structure also indicates that temperature-dependent lattice expansion is also important for this structure. We expect that further study of the this system using the quasiharmonic approximation may be useful for future study.
[24] The Mercury software package is developed at the Cambridge Crystallographic Data Centre, Cambridge, United Kingdom, available at the website http://www.ccdc.cam.ac.uk/mercury

[25] P. Hohenberg and W. Kohn, Phys. Rev. **136**, B864 (1964).

[26] W. Kohn and L. J. Sham, Phys. Rev. **140**, A1133 (1965).

[27] P. Giannozzi, O. Andreussi, T. Brumme, O. Bunau, M. Buongiorno Nardelli, M. Calandra, R. Car, C. Cavazzoni, D. Ceresoli, M. Cococcioni, N. Colonna, I. Carnimeo, A. Dal Corso, S. de Gironcoli, P. Delugas, R. A. DiStasio, A. Ferretti, A. Floris, G. Fratesi, G. Fugallo, R. Gebauer, U. Gerstmann, F. Giustino, T. Gorni, J. Jia, M. Kawamura, H.-Y. Ko, A. Kokalj, E. Küçükbenli, M. Lazzeri, M. Marsili, N. Marzari, F. Mauri, N. L. Nguyen, H.-V. Nguyen, A. Otero-de-la Roza, L. Paulatto, S. Poncé, D. Rocca, R. Sabatini, B. Santra, M. Schlipf, A. P. Seitsonen, A. Smogunov, I. Timrov, T. Thonhauser, P. Umari, N. Vast, X. Wu, and S. Baroni, J. Phys.: Condens. Matter **29**, 465901 (2017), available from the website http://www.quantum-espresso.org

[28] P. E. Blöchl, Phys. Rev. B **50**, 17953 (1994).

[29] J. P. Perdew and Y. Wang, Phys. Rev. B **45**, 13244 (1992).

[30] M. D. Johannes and N. A. W. Holzwarth, Crystalline inorganic-solid electrolytes: Computer simulations and comparison with experiment, in *Handbook of Solid State Batteries*, 2nd ed., edited by N. J. Dudney, W. C. West, and J. Nanda (World Scientific, Singapore, 2016), Chap. 6, pp. 191–232.

[31] N. A. W. Holzwarth, A. R. Tackett, and G. E. Matthews, Comput. Phys. Commun. **135**, 329 (2001), available from the website http://pwpaw.wfu.edu

[32] K. Sarkar, M. Topsakal, N. Holzwarth, and R. M. Wentzcovitch, J. Comput. Phys. **347**, 39 (2017).

[33] K. Momma and F. Izumi, Appl. Crystallogr. **44**, 1272 (2011), code available from the website http://jp-minerals.org/vesta/en/

[34] A. Kokalj, J. Mol. Graphics Modell. **17**, 176 (1999), code available at the website http://www.xcrysden.org

[35] The MathWorks, Inc., Natick, Massachusetts, USA.

[36] XMGRACE is a two-dimensional plotting software package maintained at the webpage http://plasma-gate.weizmann.ac.il/Grace

[37] M. Abramowitz and I. A. Stegun (eds.), Elementary analytical methods, in *Handbook of Mathematical Functions* (Dover Publications, Inc., New York, 1965), Chap. 3.

[38] S. Baroni, P. Giannozzi, and E. Isaev, Rev. Mineral. Geochem. **71**, 39 (2010).